Wieland, M., Pittore, M., Parolai, S., Zschau, J., Moldobekov, B., Begaliev, U. (2012): Estimating building inventory for rapid seismic vulnerability assessment: Towards an integrated approach based on mulit-source imaging. - Soil Dynamics and Earthquake Engineering, 36, 70-83

DOI: 10.1016/j.soildyn.2012.01.003

Estimating building inventory for rapid seismic vulnerability assessment: towards an integrated approach based on multi-source imaging

M. Wieland*[,1], M. Pittore[1] , S. Parolai[1] , J. Zschau[1] , B. Moldobekov[2] and U. Begaliev[3]

[1] *Helmholtz Centre Potsdam GFZ German Research Centre for Geosciences, Helmholtzstraße 7, 14467 Potsdam, Germany*

[2] *Central-Asian Institute for Applied Geosciences CAIAG, Timur Frunze Rd. 73/2, 720027 Bishkek, Kyrgyzstan*

[3] *International University for Innovation Technologies IntUIT, Gorky Street 1/17, 720048 Bishkek, Kyrgyzstan*

*Corresponding author. Tel.: +49 331 288 1283; E-mail adress: mwieland@gfz-potsdam.de

Abstract

We propose an integrated approach to estimating building inventory for seismic vulnerability assessment, which can be applied to different urban environments and be efficiently scaled depending on the desired level of detail. The approach employs a novel multi-source method for evaluating structural vulnerability-related building features based on satellite remote sensing and ground-based omnidirectional imaging. It aims to provide a comparatively cost- and time-efficient way of inventory data capturing over large areas. The latest image processing algorithms and computer vision techniques are used on multiple imaging sources within the framework of an integrated sampling scheme, where each imaging source and technique is used to infer specific, scale-dependent information. Globally available low-cost data sources are preferred and the tools are being developed on an open-source basis to allow for a high degree of transferability and usability. An easily deployable omnidirectional camera-system is introduced for ground-based data-capturing. After a general description of the approach and the developed tools and techniques, preliminary results from a first application to our study area, Bishkek, Kyrgyzstan, are presented.

Keywords: Earthquake; Vulnerability; Remote Sensing; Computer Vision; Omnidirectional Imaging; Central Asia; Bishkek

1 Introduction

Rapidly growing spatial concentrations of people, infrastructure and financial values in earthquake prone areas over the last decades have lead to drastically increased seismic risk [1]. In particular, in developing countries, such as many Central Asian countries, rapid urban growth is often accompanied by unplanned and highly vulnerable settlements, which dynamically change over short time-scales (a few years). This short time-scales, in combination with the large spatial extent and fragmentation over which the modification to vulnerability scenarios occur, represent a great challenge for local governments, which are often unable to continuously update the exposed building stock in order to adjust disaster risk reduction efforts accordingly. Therefore, an efficient vulnerability model should be able to cope with the increasing spatio-temporal variability of the dynamics of urban areas in order to successfully contribute to the main seismic risk model [2].
Commonly used procedures to analyse building inventory with respect to its vulnerability, such as a thorough (inside and outside) building-by-building analysis by structural engineers [3], may provide

high quality vulnerability information, but can not adequately cope with the rapidly changing spatio-temporal conditions in many present-day cities [4]. On the other hand, an approximate evaluation computed on a much broader scale, for instance based on census data, provides only a rough estimate of the average vulnerability and does not allow small-scale hazard information such as local amplification effects to be exploited. As a result, inventory data and thus vulnerability data is often out-of-date, spatially fragmented or highly aggregated. Therefore, there arises the need for new approaches to estimating building inventory in a rapid, standardized, transferable and comparable manner. This need is furthermore underlined by the fact that also within the Global Earthquake Model (GEM) there is a global component focusing explicitly on the development of new tools for inventory data capture [5].

Many features that can influence the seismic performance of a building are visible from the outside, and can therefore be captured remotely by images and be quantified using a visual assessment. Within this context, satellite remote sensing shows great potential for rapid vulnerability assessment over various spatial and temporal scales, covering large geographical areas at comparatively low costs. Previous studies have largely focused on techniques for extracting building footprints from high-resolution optical satellite imagery (e.g. Quickbird, Ikonos) [6,7]. Other satellite sensors have been sparsely tested for their applicability to inventory estimation for vulnerability assessment and only a few studies have used remote sensing to develop a comprehensive multi-parameter database of inventory features [8]. In this context, the potential of multi-sensor and multi-scale analysis, which combine satellite images of different types and geometrical resolutions, needs to be further explored [9,10]. A pure satellite remote sensing approach has limitations in that it is only capable of providing information about vulnerability-related features that can be assessed from the top view. To provide a comprehensive analysis of structural vulnerability, analysis of the façades of buildings should also be taken into account. Omnidirectional imaging can provide the necessary street view and shows great potential for georeferenced information extraction [11,12]. Nevertheless, its potential is still not fully tapped and further research is neccessary to improve its applicability for building feature extraction in the context of seismic vulnerability assessment. Integrated approaches, which combine satellite and street view data are rare and have so far mainly focused on image-capturing rather than on feature extraction [13].

In this paper, we propose a new approach to the estimation of building inventory as basis for seismic vulnerability assessment which is able to cope with the spatio-temporal dimension and dynamics in present-day cities. The novelty of the approach is that it combines multiple imaging sources and techniques from satellite remote sensing and omnidirectional imaging within the framework of an integrated sampling scheme, where each imaging source is used to extract specific, scale-dependent information. In an initial top-down analysis step, processing flows downwards from block scale (medium-resolution satellite images) to building scale (high-resolution omnidirectional and satellite images). Across this pyramidal searching, only the necessary data is acquired, processed and the focused geographical extent is narrowed. The aim is to minimize acquisition costs and processing time and to guide more detailed building-by-building surveys. The analysis of high-resolution satellite and omnidirectional images allows for a detailed quantification of vulnerability-related inventory features on a building-by-building basis whereas the analysis of medium-resolution satellite data is used to detect homogeneous urban structures at block scale and to identify representative sample areas for the high-resolution analysis. Therefore, in a subsequent bottom-up analysis, the high-resolution information (extracted from the identified sample areas) can be extrapolated to the corresponding homogeneous urban structures. This leads to an improved level of detail of inventory information at block scale and can provide a comprehensive vulnerability dataset for a whole city. As a case study, we present our results of applying this technique to Bishkek, the capital of Kyrgyzstan.

2 Outline of the approach

Our approach is based on a *multi-stage stratified sampling* (Fig. 1). We focus on two different levels of scale, which we will refer to throughout this article as *building scale* and *block scale* (Table 1). At building scale, any information will be defined at the most detailed level, while at the broader

block scale, we will usually refer to aggregated information.

Table 1. Considered spatial scales, corresponding available input data and vulnerability-related features.

Scale	*Description*	*Input data (Imagery)*	*Vulnerability-related features*	*Assessment*
Building	Small scale, detailed information	High-resolution from satellite or airborne, ground-based from omnidirectional	Construction type, building-footprint, area, shape, height, number of storeys, age, use, etc.	Local
Block	Medium scale, partly aggregated information	Medium-resolution from satellite	Landuse / landcover, age of built-up areas	Regional

We propose on the block scale, a regional assessment of urban structures on the basis of medium spatial but high temporal and spectral resolution satellite images (see Chapter 3). Using image segmentation, multi-temporal change detection and machine-learning based image classification, the urban environment can be delineated into areas of homogeneous urban structure, which define the strata composing our stratified sampling scheme. For each stratum, a simple random sample is drawn, whose size is chosen following a proportional allocation scheme, as described in Chapter 4. The block scale is particularly suitable for most of the subsequent stages towards the analysis of the building inventory and thus the assessment of its vulnerability, since it provides a meaningful aggregation of the exposed stock information based on physical factors, therefore potentially reducing the estimation error. Moreover, such an aggregation could greatly reduce the computational burden usually associated with risk and loss assessment for cases where the exposed inventory involves a large portfolio of buildings.
Inside the identified sample areas, a more detailed local assessment on building scale is carried out using high-resolution omnidirectional and satellite images. The analysis of ground-based omnidirectional images provides a street view of the objects of interest and therefore allows the extraction of detailed building features such as building-height, vertical shape or detection of soft-storeys. Additional vulnerability-related features can be extracted from high-resolution satellite images, which provide the top view of the objects of interest. A rapid data acquisition and analysis based on omnidirectional imaging is described in Chapter 5. Given the assumption that each stratum is composed of homogeneous urban structure, the extracted vulnerability-related inventory features can be back-propagated from building scale to block scale using the corresponding stratum as a basis.
Due to the type of input data and standardized analysis techniques, the approach can deliver comprehensive inventory data over large areas, with consistent quality. It can therefore provide a transparent and comparable data basis for vulnerability assessments, which can be applied over various scales to different urban environments.

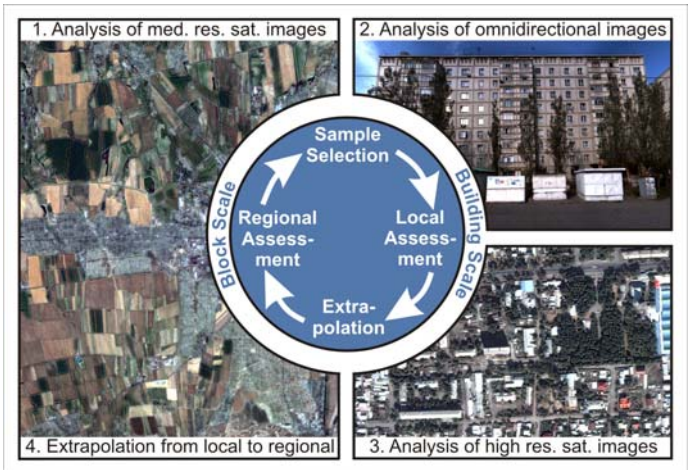

Fig. 1. Outline of the approach to multi-scale inventory data capture for rapid seismic vulnerability assessment.

3 Analysis of urban structures on block scale from remote sensing

'Urban structure types' are groups of buildings, open spaces and streets, which form a unit since they show strong similarities in the three components. Urban structure types are in the following defined as spatial units on block scale, which are homogeneous in medium-resolution satellite images in terms of their physical appearance (landcover) and usage (landuse) as well as their approximate age. The delineation of a city into areas of homogeneous urban structure types aims at creating the strata for the identification of representative sample areas for the detailed analysis of the building stock with high-resolution satellite and omnidirectional imaging. It can furthermore provide an estimate of the value and distribution of crucial vulnerability indicators at the block scale, such as predominant building-types and building-ages. The analysis of urban structures via remote sensing at block scale is carried out in three successive stages of stratification (Fig. 2).

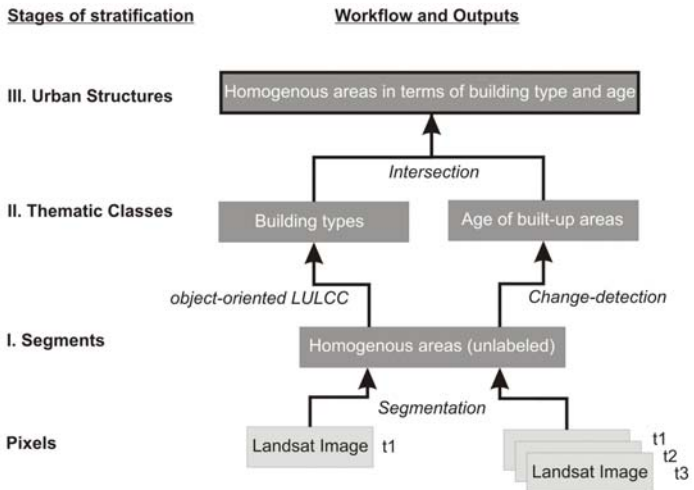

Fig. 2. Analysis of urban structures from medium-resolution satellite images.

The input data used for this analysis are images from the Landsat Thematic Mapper (TM) and Multispectral Scanner (MSS), with 30 m spatial resolution for TM and 60 m for MSS. Landsat TM data covers a spectral range of 0.45-2.35µm in 6 bands, whereas MSS data covers a range of 0.5-1.1µm in 4 spectral bands. Both satellite sensors have a large swath-width of 185 km, which allows for capturing a city as a whole within one or a few images. Furthermore they are characterized by a high temporal resolution with repeat periods of 16 days, global coverage and a publicly accessible image archive which dates back until 1972 and is free-of-charge.

3.1 Segmentation

The first stage of stratification is image segmentation. The segmentation outlines areas in the satellite image, which are homogeneous in terms of their spectral response. These areas cluster the original image pixels into *segments*, based on similarity criteria. Ideal segments are considered as singular entities composing the image (sometimes also called *superpixels*), but they can provide additional information compared to a single pixel. Geometrical and textural information can be derived from segments and later be used as additional input features for further processing [14].
In this study we use an efficient graph-based image segmentation algorithm developed by Felzenzwalb and Huttenlocher [15]. The brightness values of the image pixels in the six spectral bands of Landsat TM are taken as input features for segmentation. It should be commented that the brightness of a pixel refers to a 6-dimensional vector containing the intensity of the pixel (usually an integer in the range 0-65535) in each of the 6 spectral bands. The segmentation algorithm is based on selecting edges from an undirected graph, where each pixel represents a node in the graph, and the neighbouring pixels are connected by edges. The dissimilarity between pixels is measured by weights on each edge. As an edge weight function, we use the L2 euclidean distance in the 6-

dimensional space spanned by the spectral components of pixels connected by an edge. The algorithm therefore measures the evidence for a boundary between two regions by comparing the brightness differences across the boundary with those between neighbouring pixels within each region. A single parameter *k* conditions the average size of the resulting segments, therefore defining the scale of analysis [15]. Appropriate parameter values have been selected on a trial-and-error-basis using visual scene interpretation. The algorithm is computationally efficient and has the ability to preserve detail in low-variability image regions while ignoring detail in high-variability regions. It is therefore highly applicable to remotely sensed images, which are usually rather computationally intensive and characterised by image regions of diverse variability. The segmentation of the Landsat images is fully automated. A more detailed description of the segmentation algorithm can be found in [15].

3.2 Landuse / landcover (LULC) classification

In the second stratification stage, the segments are labelled with their predominant landuse / landcover (LULC) and approximate age of built-up areas. Object-oriented LULC classification provides information about the predominant building types. The predominant building type can be seen as proxy for the vulnerability of an area, which can be extracted from medium-resolution satellite images at block scale, and is therefore an important information layer, that can help to find suitable sample areas for the high-resolution analysis of earthquake vulnerability at the building scale.

Within a supervised classification framework, we use a support vector machines (SVM) statistical learning algorithm to label the segments according to the desired LULC classes [16]. Among the most commonly available supervised learning approaches (neural networks, logistics regression, decision trees to name only a few), SVM has been chosen because it is a well known and mathematically sound technique, able to determine the optimal decision boundaries that partition the feature space according to the properties of selected training samples [17].

When training the SVM´s model, training samples for each LULC class are manually selected based on ground-truth information. In general, the information comes from experts, who are familiar with local building construction, from visual interpretation of high-resolution aerial and satellite images or from the interpretation of ground-based GPS-photos. During the training phase, the optimal SVM parameters are selected automatically according to a standard k-fold cross-validation method. The training samples are randomly split into ten-fold subsets, where one subset is used to train the model and the others form the test samples. An optimal SVM parameter selection is reached when the cross-validation estimate of the test samples error is minimal. Using a k-fold cross-validation moreover further decreases the risk of over-fitting [18].

The feature vector describing any segment to be classified is composed of 26 components, which include the mean and standard deviation of the spectral values for the 6 Landsat bands, the mean and standard deviation of the Normalized Difference Vegetation Index (NDVI) [19] and 2 band-specific texture descriptors derived from the Gray-Level Co-occurrence Matrix (GLCM) computed over the segment [20]. The texture descriptors take into account neighbourhood relations between pixels, and are of particular importance when analysing the urban landscape, where LULC classes are mainly defined by the visual pattern of buildings, streets and open-spaces. All descriptors of the feature vector are calculated separately for each segment.

To ensure a higher degree of transferability of the method, a classification hierarchy is set up. The hierarchy consists of three levels of increasing spatial resolution (l_1, l_2, l_3) that give step by step guidance to find the number and value of classes that best fit a specific study area. For l_1 the four classes 'urban / built-up land', 'vegetation', 'water' and 'other (rocks, bare soil, etc.)' are distinguished. Because the focus of our approach is urban built-up areas, only the class 'urban / built-up land' is further refined and split into more detailed classes in l_2 ('residential', 'industrial / commercial', 'mixed built-up land') and l_3 levels. The classes in l_1 and l_2 are fixed and can be

applied to any study area worldwide, whereas the l_3 classes are dynamic and are dependent on the specific study area and existing local building classifications (see Fig. 5 for the l_3 classes defined for the study area).

3.3 Multi-temporal change detection

The age of built-up areas is the outcome of a multi-temporal change detection. Change detection is a process that identifies spatio-temporal differences in the state of an object by observing it at different times. It allows for detecting if a change has occurred, identifying the direction, quantifying the spatial extent, and assessing the spatial pattern of the change [21]. To assess changes in the urban environment and therefore obtain information about the approximate age of built-up structures, we use multi-temporal change detection based on a quantitative analysis of Landsat TM and MSS images, which cover the same spatial extent but are taken at different times.
Among the different change detection methods available, post-classification comparison was chosen, as it directly provides not only information about the spatial distribution and rate of change, but also about the change direction [21,22]. Within this change detection method, LULC classifications that distinguish built-up from non-built-up areas for the individual Landsat images are compared on a pixel-by-pixel basis and a change matrix is generated. This change matrix provides the 'from-to' information of every LULC class, which allows for identifying and analysing changes. The accuracy of this change detection method depends mostly on the accuracy of the individual LULC classifications of input images.
LULC classification for each input image is carried out using the same approach described in Chapter 3.2 with l_1 as the scale of classification hierarchy. A more detailed level of classification, which further divides the urban areas according to their use, is not necessary for an analysis of the age of built-up structures in general. In fact, a more detailed classification could result in a decrease of the overall accuracy, as the selection of high-quality and sufficiently numerous training samples gets more difficult with increasing numbers of classes, in particular for historical image data [21].
After implementing the post-classification comparison, the generated change matrix is prepared in a way that only changes of the urban built-up structures are highlighted. By analysing the changes between the different acquisition times of the input images, the approximate age of built-up areas can be derived. The age of built-up structures is of particular interest when selecting sample areas for a more detailed seismic vulnerability assessment, because seismic building codes and construction practises change over time and can significantly influence the vulnerability of structures. Therefore the age of built-up structures is often considered as additional proxy when assessing their vulnerability for example according to the European Macro-seismic Scale (EMS-98) [23].

In the third stage of stratification, the LULC classification is combined with the age of built-up areas into a new thematic layer by spatial intersection. The final output of this stage is thus the partitioning of the urban environment into *urban structures types*, which are at block scale homogeneous in terms of LULC and approximate age. This thematic layer represents the final strata for sampling.

4 Sampling and routing for efficient omnidirectional imaging surveys

A careful identification of sample areas for a more detailed analysis of the building stock is important in order to achieve the best trade-off between observation area, acquisition time and costs. To allow for better efficiency of ground-based data-capturing, street data inside the sample areas is also taken into account. Optimal driving routes, which cover all the streets inside the sample areas using the shortest-path, are calculated for easy and rapid in-field navigation.

4.1 Sampling

From a statistical point of view, estimating inventory information at block scale can be regarded as the problem of estimating an unknown *population* [24]. Usually estimation is based on a *sampling frame*, which defines the composition of the population, how to draw samples from it and what kind of information each sample is composed of. Let us observe that the considered population has the following attributes:

1. It is functionally dependent on several physical attributes of the building stock.
2. It can be estimated at building scale by visual observation.
3. It can be approximated by a spatial function of the geographical position.

Therefore, in our sampling frame, we will draw samples from the building population, where each sample will involve the measure of several physical attributes of the selected buildings (at building scale). Different sampling methods are in principle available: *systematic sampling* or *simple random sampling* (SRS) for instance would provide a reasonable scheme in absence of any other information. We know, nevertheless, that the population of interest is connected to the composition of the urban morphology, thus will likely exhibit a great variability related to LULC, the time of construction of the buildings and other social and economic parameters. An estimate based on a simple random sample would be affected by such variability in term of precision and mean square error. In this case, a stratification of the sampling would instead achieve a much greater precision, provided that it is possible to suitably partition the population into sub-populations as homogeneous as possible with respect to the features of interest [24]. In stratified sampling the samples are drawn from different disjoint subsets of the population, called *strata*, instead of from the sampling frame as a whole. In our approach, the urban structure types form the strata for sampling. Therefore, for each urban structure type, a simple random sample is drawn.
The actual sampling process is based on a *proportional allocation scheme.* Proportional allocation is important in order to obtain an unbiased estimate of the features of interest, and to ensure that sub-populations of different size will be evenly represented in the sampling process [24]. In a first step the largest segment of each stratum is selected for a closer inspection. The selected representative segment is then further analysed in a second step to define the final sample area for the related stratum. Preference is given to square-shaped sample areas due to shape-constraints in the data ordering process for high-resolution satellite images, which are used for a local assessment. The location of the sample area inside the representative segment is chosen randomly. The algorithm designed to calculate the sample areas takes a minimum and maximum threshold for the desired size of a sample area as input values, which are defined proportional to the stratum size. To determine the sample size for a desired level of statistical reliability the Coefficient of Variation (CV) is used [25]. Due to a lack of information about the actual composition of the building population from previous surveys, a CV for each stratum is first approximated from the mean and standard deviation of the brightness values of the Landsat image. Variations in the image reflect the underlying urban structure, but more detailed conclusions about the composition of the building population can not be drawn only from the image information and the actual building population may have a larger variability. Therefore, the largest CV approximated from the image information is used for the calculation of the minimum size threshold. To account for a possibly larger variability of the building population the maximum size threshold is set to the stratum size. Choosing a range of acceptable sample sizes allows for giving tolerance to the sampling size while giving preference to the sampling shape. If a maximum sized, square shaped sample does not fit into a segment at the randomly selected location, another location is chosen until the sample area fits. If no location can be found inside the representative segment for the desired sample size and shape, the sample size is linearly reduced by 1 m^2 and the location search is repeated. These steps are iteratively carried out until a square sized sample fits into the segment or until the minimum size threshold is reached. If the minimum threshold is reached and a sample area still does not fit into the segment, the whole segment will be taken as sample area.

The representative sample areas, which are automatically identified by this procedure, form the spatial extent for a detailed local assessment of the building stock with high-resolution satellite and omnidirectional imaging on building scale.

4.2 Routing

Once representative sample areas are identified, optimal driving routes for a ground-based omnidirectional imaging survey need to be calculated within these areas. An optimal route within the context of this study means a driving path which covers all street-segments in the sample areas with the shortest overall driving length. Calculating routes in advance aims to reduce the overall driving length of a ground-based survey and therefore to minimize costs and time for the field-trip. Furthermore, data gaps and overlaps can be reduced and therefore disk space can be optimized by avoiding the capture of redundant data.
We use freely available georeferenced street-data in digital vector-format from OpenStreetMap (OSM) as a basis for the routing. OSM is a free editable map of the world that aims at creating and providing free geographic data, such as street maps [26]. OSM works after the 'wiki-principle', which means that quality assessment of the content is assured by the self-regulating mechanism of a user community. Contributors to OSM bring in their local knowledge and create and edit geographic data by digitizing from aerial images (provided by OSM) or by GPS tracking. Because the quality and completeness of the provided data vary from place to place, a final check of the desired dataset and its topology is needed and manual corrections or extensions may be necessary before using OSM data. The cleaned and updated street vector data is then used to create a routable geometric network with cost-factors for travelling along a specific street-segment. The major cost-factor used is the length of a street-segment, but also additional cost-factors and restrictions, such as street quality, turn restrictions, traffic information, etc., can be added to the network if available.
In the context of this study, the routing problem can be reduced to the common Travelling Salesman Problem (TSP). The TSP is a well-studied combinatorial optimization problem, in which a traveller is required to minimize the total travelling distance in order to visit all the stops on his list only once [27]. As we want to cover all street-segments inside each sample area, stops are set at the central, start and end node of each street-segment. To solve the routing problem we use the ArcGIS 9.3 network analyst route solver tool. The underlying algorithm determines the best route through a series of stops with a minimum cost by using a modified Dijkstra algorithm [28]. The calculated routes are used during field-surveys in combination with real time GPS-tracking to navigate the car with the omnidirectional imaging system through the pre-selected sample areas in the most efficient way.

5 Ground-based omnidirectional imaging

In the last few years omnidirectional imaging has increasingly gained attention, boosted by applications such as Google StreetView, which clearly showed how powerful this technique can be in aiding people to visually explore an unknown environment [11].
Omnidirectional images are projections of a spherical field of view onto a central point [29]. Therefore, their natural representation should be a curved manifold [30]. Due to the inherent difficulties in handling and processing such a structure, omnidirectional images are usually mapped onto a planar, equirectangular representation. This mapping, also known as *plate carrée*, is an equidistant cylindrical projection that maps meridians onto equally spaced vertical straight lines, and circles of latitude into equally spaced straight horizontal lines [31]. This representation can be processed as a conventional image, taking into account that the spatial resolution of the image is different from point to point and that there is a strong distortion around the poles. The equirectangular representation is widely used, mostly due to the very simple relationship between the location of a point on the map and its corresponding location on the sphere that has been mapped [32].

Omnidirectional imaging is particularly convenient for any application related to environmental modelling [12,30], in particular due to the following reasons:

1. Capturing all at once a very wide (360°) field of view means that there is no need to choose what to capture. Were a conventional camera to be used instead, the operator would consider a number of choices, favouring for instance certain buildings or not following them enough to capture important details. This could bias the outcomes of the survey and also affect the overall speed of the survey operation.
2. There is no need of experienced operators, and the whole image capturing process can be performed almost automatically by simply driving around an area of interest with the system fixed onto the roof of a car. The system is easily mounted on different car types and can be monitored by an operator inside the car. Therefore, such a system can be deployed and operated very easily and extensive surveys can be performed in a reduced amount of time.
3. In the perspective of an automated analysis and interpretation of the images, the extended field of view of the omnidirectional camera allows for the more robust detection and tracking of geometrical features that can be used to infer 3D characteristics of the objects depicted.

The system is basically composed of a camera, a GPS receiver and a laptop. A simple yet effective mounting system, featuring a light-weight aluminium frame and 4 high-power suction cups, allows the rapid and easy mounting on different cars. A Ladybug3 omnidirectional camera from Point Grey Research Ltd. made up of 6 colour CMOS cameras has been selected. The camera has a single ieee-1394B interface link for high-throughput data capturing. Image sequences described in this paper have been captured at a sampling rate of 10 Hz, full resolution (5700x2700 pixels) colour JPEG format. The GPS receiver includes a low-cost, patch antenna and a small board connected via USB to the laptop, and provides positions with a 1 Hz sample rate. Position is then associated to each frame of the sequence by interpolation of available GPS data using b-splines. A custom software application has been developed to capture, synchronize and save the different data streams. The synchronization of the data is based on the high-quality timer embedded in the ieee-1394B hardware controller, which provides a basic 125 microsec time-frame, reasonable for our purposes.

5.1 Automated estimation of building height from omnidirectional imaging

Image processing applied to omnidirectional imaging is a potential source of information related to seismic vulnerability. As a matter of fact, many features that can influence the seismic performance of a building are visible from the outside, and are therefore subject to quantification by means of a suitable, possibly automatic, visual assessment. Among such features we can (not exhaustively) mention height, number of storeys, presence of weak/soft storeys, number and distribution of openings (windows and doors), 3D shape, symmetry and distribution of vertical and horizontal elements.

An extensive assessment of the application of advanced computer vision techniques to the task of automatically extracting such features from an omnidirectional image stream is currently in preparation. In the following, we will describe a proposed processing pipeline for inferring information about the *height of a building*, assuming that we know its position. Let us consider, inside a longer sequence, three omnidirectional images captured sequentially, and assuming that one or more buildings are visible in the sequence. GPS-based positioning is available for each frame of the sequence. Since the camera is moving while capturing the images, each available frame will represent a coordinate reference frame encoding a different point of view. By computing the optical flow, the vector field describing the apparent displacement of each pixel between two images is obtained [33], providing spatially dense information about the 3D structures visible in the images [34]. In order to achieve this, we compute the optical flow first on the frames f_0, f_{+1} and then on

the couple f_0, f_{-1} . The two different vector fields, combined, describe the apparent displacement of each pixel from frame f_{-1} to frame f_{+1} . Therefore for any point $\boldsymbol{p}_a$ in the frame f_{-1} , a displacement vector is computed which maps to a point $\boldsymbol{p}_b$ in the frame $f_{\square 1}$ (Fig. 3). We consider three frames (instead of two) in order to obtain a longer baseline T (defined as the actual distance between two observation points), therefore reducing the uncertainty in the evaluation of the 3D coordinates.

If we suppose that most of the image pixels are related to fixed structures (typically buildings), we can use their apparent displacement to compute the change in pose (rotation) and the displacement (translation) of the camera between the two frames [32]. The matrix which encodes this information is called the essential matrix [33] and can be computed by the set of correspondences provided by the combined optical flow fields [35]. The two matrices explicitly describing rotation and translation are then extracted from the essential matrix following the method described by Horn [36].

As pointed out by Horn [36], the resulting translation matrix is defined up to a scale factor, therefore we need a calibration factor to obtain metrically valid estimates. The calibration factor is provided by the absolute magnitude of the real displacement of the camera, provided by comparing the GPS position of the considered frames.

Once we have successfully characterised the 3D transformation binding the two reference systems, we can obtain the 3D coordinates of the (real) points that have been mapped onto the image pixels by applying a suitable triangulation. For each couple of pixels $\boldsymbol{p}_a$, $\boldsymbol{p}_b$ above defined, using the already computed 3D transformation, we define two lines stemming from the two centres of the projections (the origins of the two reference systems related to the two positions of the camera) and passing by the 3D point on the surface of the sphere related to the pixel coordinates in the images (Fig. 3).

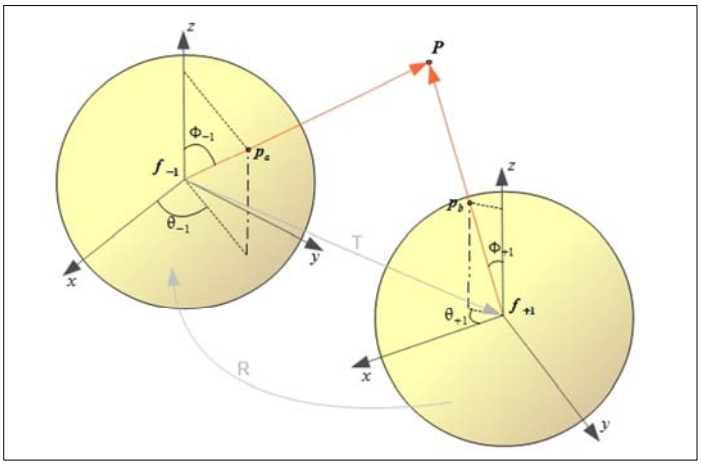

Fig. 3. Two omnidirectional frames are represented as spherical images whose centres and orientations define two reference systems. The positions of the centres are given by GPS positioning and take into account the movement of the camera while acquiring the images.

The two lines would theoretically cross in the 3D position of the point that generated the two projections. Due to the inherent uncertainties, the lines are not likely to exactly cross, but it is common to define the crossing point as the median point of the minimal segment joining the two lines. The reconstructed 3D point $\boldsymbol{p}$ is defined in the reference system of the camera at frame f_{-1} . Since we know the coordinates of the centre of projection and the orientation of the camera in the external coordinate reference frame (by the GPS information embedded in frame f_{-1}), we can describe the point $\boldsymbol{p}$ in a common reference system, G where a sparse grid is defined.

The considered grid is defining a Cartesian coordinate system G , depicted in Fig. 4. The reconstructed 3D points are instead defined within a moving coordinate system attached to the camera, and indicated as G in Fig. 4. (for sake of simplicity all reference systems are considered

two-dimensional for positioning purposes). The two reference systems are linked by the simple relationship:

$$\vec{P}_G = R^{-1}\vec{P}_C + \vec{T} \quad (1)$$

Where $\vec{T}$ and R are respectively the translation vector and the rotation matrix between the grid and the camera reference systems, and $\vec{P}_C$ and $\vec{P}_G$ are the horizontal projections of the same 3D point in the two coordinate systems. The origin of the camera system is located in its optical centre, and its direction is defined by the *versor* of the instantaneous velocity vector, as computed from the camera GPS trajectory. Once the coordinates of the point are defined in the G reference system, the active element of the grid G_{ij} is selected and the measurement is added (Fig. 4).

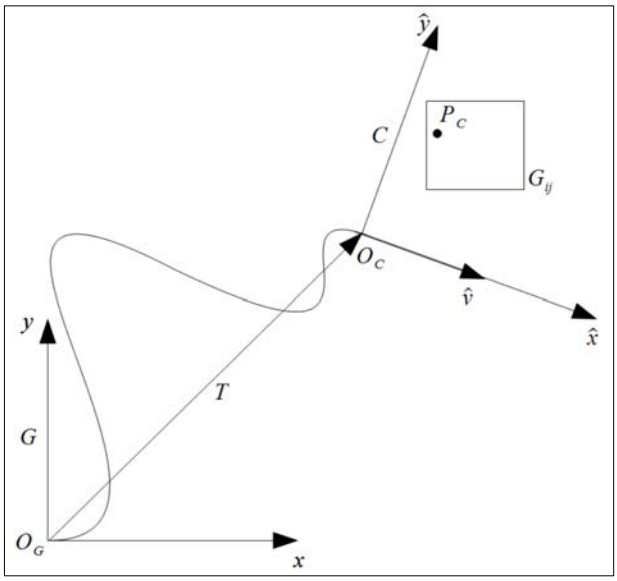

Fig. 4. The different coordinate reference systems (RS) considered; G is the Grid RS, C is the Camera RS, oriented according to the instantaneous camera velocity versor. The curved path represents the camera trajectory. The square G_{ij} represents the i,j element of the grid, where the measurement with horizontal coordinates $\vec{P}_C$ would be stored.

For sake of simplicity, we consider each reconstructed 3D point as a single measurement, and aggregate all measurement in the grid spanning the area of interest. Every cell of the grid, by default of size 10m, will be given a value depending on the measurements falling in the cell. The value is obtained by computing the cumulative histogram of the z-component $\mathbf{z}_i$ of the 3D points $\mathbf{p}_i$ falling in the cell, where the bins range from $max(\mathbf{z}_i)$ to $min(\mathbf{z}_i)$, and choosing the first bin whose occupancy is over a threshold (usually from 20 to 40 pts). Such a threshold is useful to filter out outliers or 3D points related to punctual features such as, for instance, antennas or small chimneys.
Depending on the quality of the 3D reconstruction, the step of the grid can be changed in order to consider extracted features at a different scale. Since we focused on the height of the buildings as the most significant geometrical parameter related to vulnerability, a coarse grid has been chosen to filter out high-frequency noise in the measurements.
If the position of a building is already known, for instance resulting from the manual or automatic analysis of high resolution satellite images, the 3D measurements can be used to assign the most likely height to the building. This is accomplished by taking the average value of the non-empty grid elements overlapping the building, if the footprint is available, or just the one containing the building location if specified by a point.

5.2 From building inventory to seismic vulnerability

If significant inventory features are available for one or more buildings (e.g. construction type,

building age or building height) an estimate of their seismic vulnerability is possible. Different approaches have been proposed to estimate vulnerability [2], and a discussion about the specific choice is beyond the scope of the present article. We just remark that often information about the building inventory is available, relating specific features with a most likely vulnerability description. Hence we can refer to those features as vulnerability proxies, and use the collected data about the inventory to infer vulnerability. Following the approach proposed in this article, for instance, it is possible to obtain an estimate of the approximate building age from the multi-temporal analysis of medium-resolution satellite images and a precise estimate of the building height for those buildings which have been captured by the omnidirectional camera. The LULC classification based on medium-resolution satellite images can furthermore give a first approximation of the pre-dominant building type of an area. A more precise estimate of the building type for a specific building can be automatically inferred from the previous parameters, where enough a-priori information is available, or manually assessed by inspecting the omnidirectional video stream. An exemplification of a procedure which links these inventory features with a local building taxonomy to classify building vulnerability according to EMS-98 is given in Chapter 6 for the city of Bishkek, Kyrgyzstan.

6 Case study: Bishkek, Kyrgyzstan

Bishkek, the capital of Kyrgyzstan, is situated in one of the most seismically hazardous zones in Central Asia. The city developed primary during the 20th century and therefore only a relatively short record of strong earthquakes in the area is available in comparison to other parts of Central Asia. A probabilistic seismic hazard assessment computed at regional scale for Kyrgyzstan confirms the high hazard of the region and shows that a peak ground acceleration of up to 4.5 m/s² has a probability of 10% to be exceeded in the next 50 years [37]. Taking into account the centralized design and construction practices in the former Soviet Union, the buildings in Bishkek are moreover highly vulnerable to earthquake hazard. A seismic risk scenario carried out on city scale for Bishkek, which considers a magnitude 7.5 earthquake occurring over the Issyk-Ata fault, estimates that 30% of the buildings will collapse and 63% of the buildings will be severely damaged [38].

A crucial part of the seismic risk assessment involves the analysis of the existing building stock with respect to its vulnerability. During a time period of five years from 1999 to 2004, a thorough inside and outside building-by-building assessment was carried out by civil engineers for central parts of Bishkek. This kind of assessment proved to be sufficient in determining the vulnerability of these buildings to earthquakes, but it is highly time- and cost-consuming and as a result the dataset is spatially fragmented and not complete. Furthermore, given the rapid growth of Bishkek in recent years, there is neither up-to-date inventory data nor vulnerability classification data available for large parts of the city. Updating the existing inventory data using a traditional civil engineering approach to provide a complete earthquake vulnerability assessment of the whole city would not be feasible due to cost and time constraints. On the contrary, the data used in Bindi et al. [38] for Bishkek is highly aggregated for the city as a whole and does not allow for a spatially more detailed vulnerability model. This lack of inventory data significantly impedes progress in seismic vulnerability and risk assessment. To overcome the lack of data, satellite- and ground-based remote sensing are proposed as a way to provide an up-to-date and realistic inventory assessment for the city of Bishkek on different scales.

An analysis of the urban environment at block scale using remote sensing has been carried out to delineate Bishkek into urban structure types. In the first stratification stage, a Landsat TM image from 08.07.2009 was *segmented* based on the brightness values in the 6 spectral bands. Superimposing the resulting segmentation output onto a high-resolution Quickbird image from 09.11.2009 allowed for a qualitative assessment of the accuracy by visual inspection (Fig. 5). Urban areas of different complexity, which appear homogeneous in terms of their spectral response in the Landsat TM image, could be outlined properly.

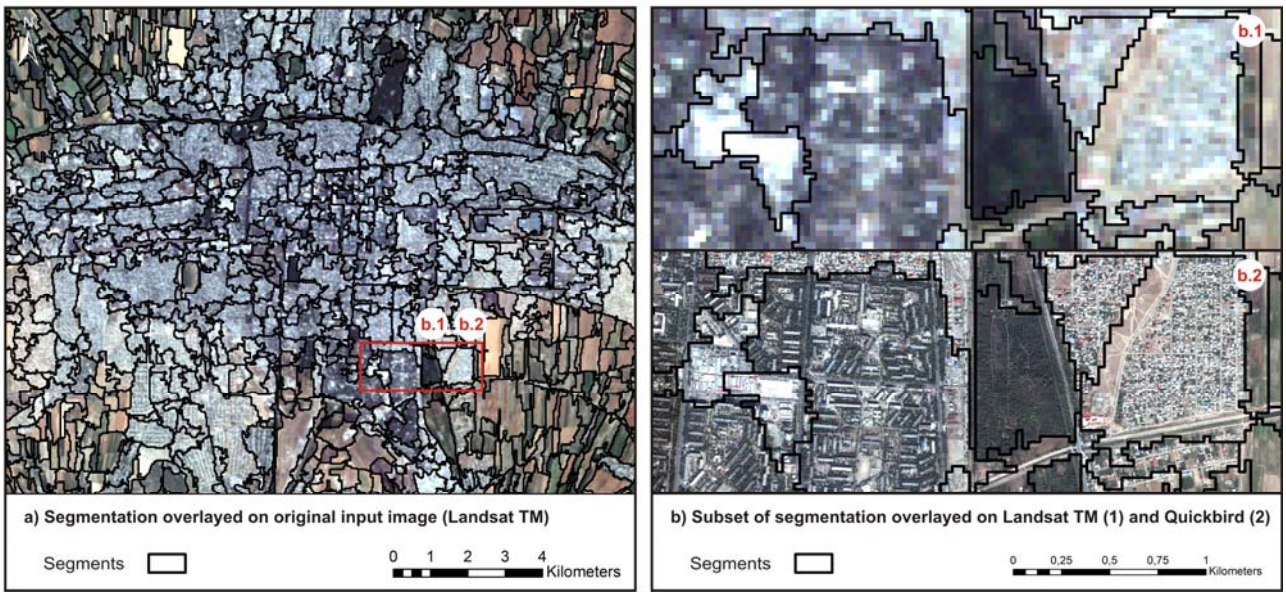

Fig. 5. Segmentation of Landsat TM superimposed on a) and b.1) Landsat TM (30 m) and b.2) Quickbird (0.6 m).

In the second stratification stage, the segments were labelled according to their *predominant LULC*. Following the classification hierarchy and taking into account expert knowledge on local building construction [39], 10 different LULC classes could be identified for the city of Bishkek (Fig. 6). A total of 200 ground-truth points have been collected by visual interpretation of GPS-photos and high-resolution aerial and satellite images from Google Earth. For each LULC class, 10 training samples were randomly selected from the ground-truth points to feed as input for the SVM learning machine. The rest of the ground-truth points have been used as test samples to assess the accuracy of the resulting classification. An overall accuracy (defined as total number of correctly classified segments divided by the total number of test samples) of 71% was assessed for the classified image. Misclassifications were mainly related to a partial overlap of the textural and spectral signatures of bare soil and rock with certain LULC classes of the built-up areas, and occurred mostly outside of the city borders of Bishkek in rural areas with large fallow agricultural fields or in mountainous areas with large patches of bare rock. These areas were falsely classified as 'industrial / commercial'. Through only minor manual post-classification refinement the overall accuracy could be increased to 81%. Covering 67.4% of the total built-up area of Bishkek, 1-2 storey masonry, brick individual apartment houses (subdivided into three different classes: low, medium and high built-up density) are clearly the dominating building type. 3-6 storey masonry, brick, concrete, panel buildings with 11.4% are the second most wide spread building type followed by 7-9 storey concrete panel, frame and monolithic buildings with 2.4% of the total built-up area. Mixed built-up areas account for 7.4%, whereas industrial / commercial areas cover 11.4% of the built-up area in Bishkek.

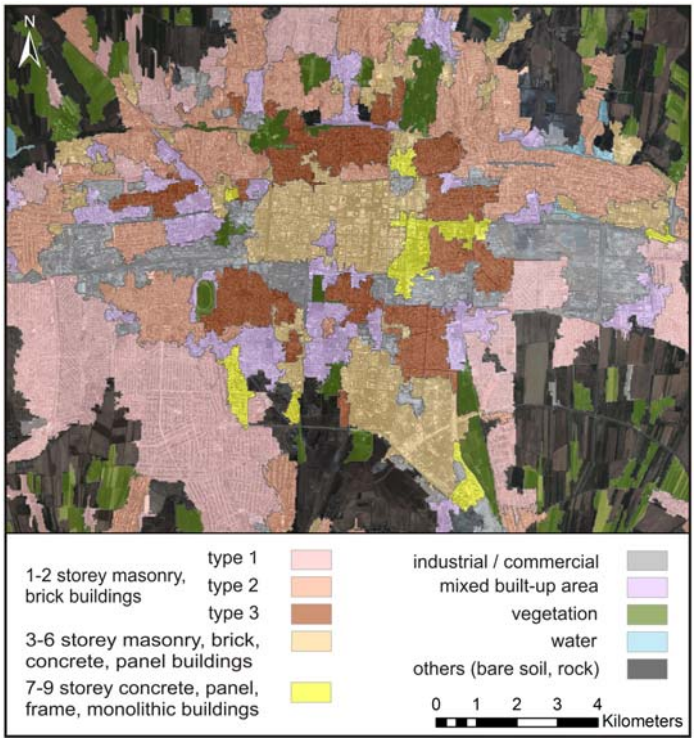

Fig. 6. LULC classification of Landsat TM image from 08.07.2009 for Bishkek superimposed on Quickbird.

Multi-temporal change detection using a post-classification comparison method was carried out to assess the approximate age of built-up areas and to obtain information about the degree and directions of urban sprawl (Fig. 7). Landsat MSS and TM images from three different time-steps (1977, 1994, 2009) covering the same spatial extent were co-registered and used as input. Due to different spatial resolutions between the sensor systems, the MSS images were resampled to 30 m resolution of Landsat TM. Every image was segmented and classified separately into the four classes of l_1 of the classification hierarchy (Chapter 3.2). Within the change detection method, the different LULC classifications were compared on a pixel-by-pixel basis and change matrices were generated for the time-periods from 1977 to 1994 and from 1994 to 2009. The change matrices provide the 'from-to' information of every LULC class, which allowed for identifying and analysing the changes of the built-up areas separately. When using a post-classification comparison, the accuracy of the change detection result depends strongly on the accuracy of the individual LULC classification of the input images. Table 2 shows the results of accuracy assessments for the three classifications based on a comparison of the individual classification with independently selected test samples.

Table 2: Accuracy assessment of the LULC classifications used as input for post-classification comparison (overall accuracy is defined as total number of correctly classified segments divided by the total number of test samples).

Image (acquisition date)	*Overall accuracy*
Landsat MSS (22.08.1977)	88,33%
Landsat TM (15.07.1994)	87,67%
Landsat TM (08.07.2009)	90,00%

In 1977 a total area of 117 km² was classified as built-up. In 1994 the built environment in Bishkek and its surroundings accounted for 152 km², while in 2009 the city reached a total built-up area of 235 km². The urban sprawl between 1977 and 1994 was mainly concentrated on the suburban eastern and northern parts of the city with an absolute growth of 35 km² (urban growth rate of 29.91%) and an annual percentage growth rate of 1.75%. Between 1994, three years after the Kyrgyz Republic became independent of the former Soviet Union, and 2009, Bishkek expanded rapidly with an annual percentage growth rate of 3.64% and an absolute growth of 83 km² (urban

growth rate of 54.60%). Most of the buildings built during that time period are residential 1-2 storey buildings of varying construction material and were constructed mainly in the southern parts expanding rapidly towards the Issyk-Ata fault system. These areas close to the fault system, where many new buildings are still being constructed, show the highest seismic hazard [39]. Large quarters have also been constructed recently in the far northern parts of the city in the direction towards the Ala-Archinskoye Reservoir.

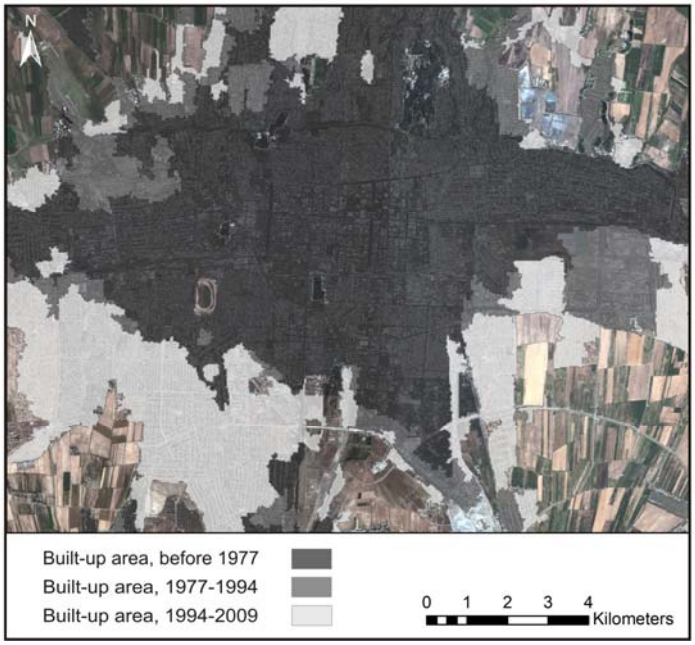

Fig. 7. Approximate age of built-up areas from post-classification comparison of Landsat MSS and TM for Bishkek superimposed on Quickbird.

In the third stratification stage, the two thematic layers of the LULC classification and the age of the built-up areas were intersected onto a new thematic layer representing *urban structure types*, which are on a block scale homogeneous in terms of LULC and approximate age. The urban structure types layer (Fig. 8) therefore provides a more detailed delineation of the city compared to the single LULC (Fig. 6) or age (Fig. 7) layers. A total of 21 urban structure types could be identified for the built-up area of Bishkek. The urban structure types consist of 7 different LULC classes of the built environment in combination with three different building age classes. Fig. 8 shows the urban structure types as well as distribution and extent of the 21 automatically identified representative samples. The total calculated sample area for Bishkek is 12.3 km².

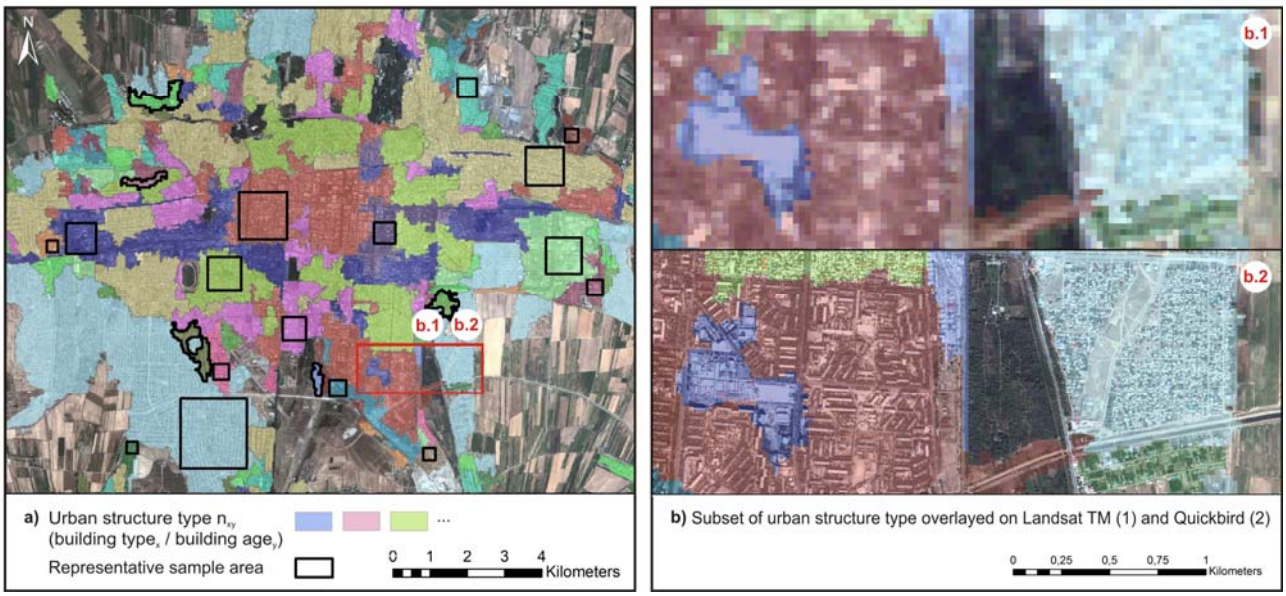

Fig. 8. Urban structure types forming the strata for automated selection of representative sample areas for Bishkek superimposed on a) and b.2) Quickbird and b.1) Landsat TM.

To guide an efficient ground-based image capturing campaign in the most efficient way, *optimal driving routes* were calculated inside the sample areas based on modified OSM street-data. The only cost-factor used in this study is the length of a street-segment. Other cost-factors and restrictions, such as street quality or turn restrictions, could not be added to the network, because this information was not available beforehand. Stops were selected automatically at the central, start and end nodes of each street-segment and the best sequence of visiting the stops was calculated for each sample area separately using the ArcGIS network analyst route solver tool. The calculated routes were then used during a field-survey in Bishkek in combination with real time GPS-tracking to navigate omnidirectional image capturing from a car through the pre-selected sample areas in the most efficient way. The calculated route length accounted for only 125 km of the overall street-length of 1468 km for the main urban area of Bishkek. This means a reduction of the observation route by 91.5% compared to the overall street-length.

During the *ground-based acquisition campaign* of one week, almost 3 TByte of georeferenced images were collected, and are currently being processed. As an example of the type of outcome that we can envisage, we provide some results from the height assessment procedure. As shown in Fig. 9, it is possible to obtain a fairly accurate 3D reconstruction of the façade of a building from three contiguous georeferenced omnidirectional frames. The 3D reconstruction is defined in the reference system of the camera relative to the first frame of the subsequence. Since we know from the GPS track the position and the orientation of the camera at the same time frame, we can define the 3D coordinates of the reconstructed points in an external reference frame. Note that in this case it would be possible to assess several different geometrical characteristics of the building from a detailed analysis of the façade. Since here we are interested in the height of the buildings, we can define a two-dimensional height distribution over a local Cartesian grid. Each cell of the grid is given a value based on the reconstructed 3D points whose x / y coordinates are inside the area spanned by the cell itself. The 3D reconstruction based on three frames can be repeated, sampling the original frame sequence at equal intervals and upgrading each time the 2D measurement grid accordingly. Fig. 10 shows the 2D height distribution superimposed on a georeferenced satellite image.

This example is representative of the quality of results that can be obtained in standard operational conditions: where buildings are mostly visible in the input images, the results from this height assessment procedure are satisfactory. Moreover, there is space for further and more advanced applications of computer vision techniques for automated extraction of vulnerability-related inventory features.

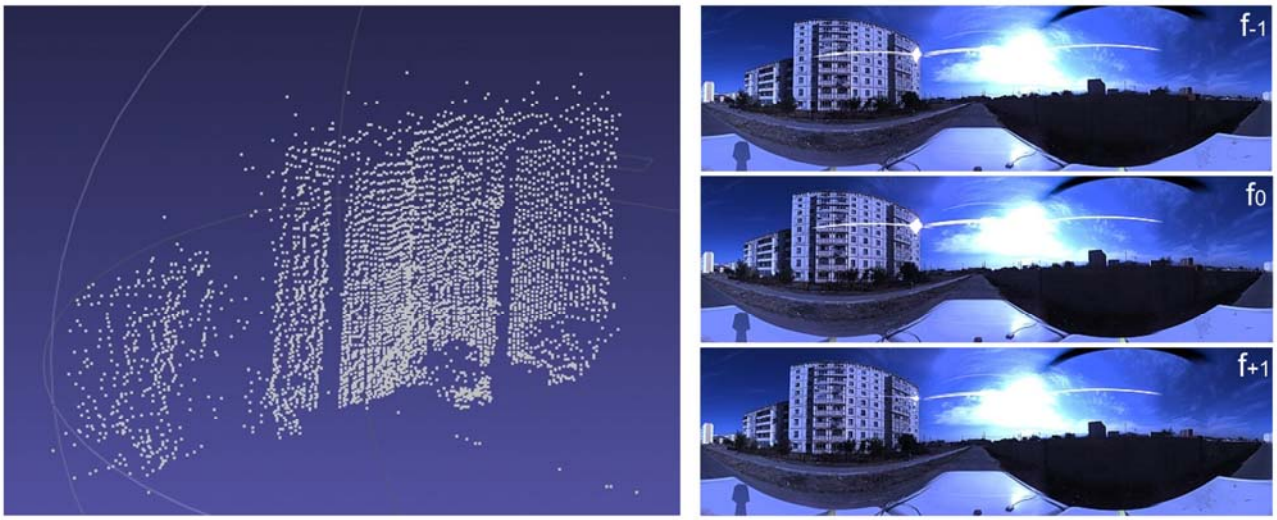

Fig. 9. 3D reconstruction of the facade of a building (left) from three contiguous frames (f_{-1}, f_0, f_1) of an omnidirectional sequence. The small step-back of the facade and the nearby building are clearly visible. At the base of the main building it is possible to notice two trees.

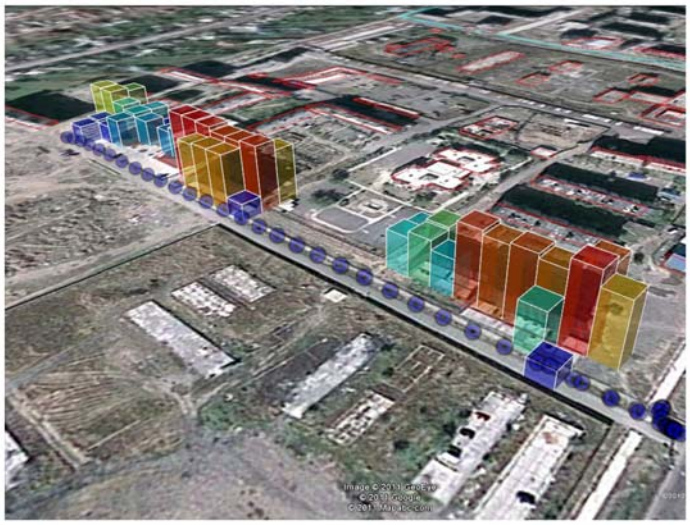

Fig. 10. The estimated heights of the buildings are mapped as a 2D distribution on a georeferenced map (source: GoogleEarth). The estimated height is consistent with the manually assessed number of storeys of the considered buildings.

An exemplification of how *seismic vulnerability* could be estimated is given in the following. The information we are starting from is the footprint of a small set of buildings, manually digitised from a high-resolution satellite image. The building footprints provide information about the buildings location and size. The buildings can furthermore directly inherit the features described by the strata they intersect, namely LULC and age. By intersecting the building footprints with the grid, that is storing the 3D measurements, it is possible to assign a height value to the building. The latter assignment is obtained by computing the weighted mean of the values in the grid cells having a non-empty intersection with the building footprint. The weight used is the normalised number of measurements in each cell of the grid. The uncertainty on the estimated height is the squared root of the weighted, unbiased variance.

The number of storeys for each considered building is estimated considering a typical storey height of 3 m and an additional 1 m of cornice / roof structure, namely:

$$n_{storeys} = \lfloor (height - 1) \div 3 \rfloor \quad (2)$$

All the data collected, estimated or inferred about the small set of buildings considered in this example are shown in Table 3. The number of storeys has been correctly estimated and even considering that no ground-truth is available for a more rigorous validation of the photogrammetry,

the estimated height values are reasonably satisfying.
A preliminary estimate of the seismic vulnerability of the buildings according to EMS-98 has been obtained by analysing the most common building types in Kyrgyzstan, as described by the World Housing Encyclopedia (WHE) [40]. For each building the most compatible building type could be selected from the WHE based on its inventory features. Finally the vulnerability class, which is most commonly associated to the selected building type (also indicated in the WHE reports) has been assigned to the specific building. As shown in Table 3, the buildings #1 and #2 (Fig. 11) are compatible with building types described either by vulnerability classes *E* or *C*. The buildings #3 and #5 are very likely to be described by vulnerability class *E*, and building #4 has been assigned vulnerability class *C* (Fig. 12, Fig. 13).
Since our purpose is to test the feasibility of an automated estimation of the seismic vulnerability, the assignment has been done purely on the basis of the available data and does not involve any engineering consideration of the specific buildings. In the case of buildings #1 and #2, further analysis or a manual assessment (for instance by inspecting the omnidirectional images of the buildings) would provide a more reliable estimate of the vulnerability. Nevertheless, it is interesting to note that in the case of the building stock of Kyrgyzstan the height of a building, or better the number of storeys, is a key parameter in order to correctly infer the specific building type. This parameter may not be directly connected to the seismic vulnerability estimation, but it is proving critical to link the considered buildings to their most likely taxonomic description.

Table 3. Example of building inventory data collected for a subset of buildings in Bishkek.

Building #	*Dimensions from digitised footprints (m, length x width)*	*LULC of area from Landsat*	*Age of area from Landsat*	*Height from omnidirectional (m, estimated ± σ)*	*Nr. of storeys from height*	*Most likely EMS-98 vulnerability class inferred from WHE*
1	25 x 18	7-9 storeys concrete panel, frame or monolithic	1994-2009	15,2 ± 1,6	4	*E* / *C*
2	25 x 21			14,7 ± 2,6	4	*E* / *C*
3	42 x 13			28,8 ± 1,6	9	*E*
4	26 x 11			17,0 ± 2,5	5	*C*
5	47 x 13			28,9 ± 2	9	*E*

Let us remark that these estimates are preliminary and mostly aim at exemplifying the possible processing steps involved and the potentials of the proposed approach in the collection of valuable information on the building inventory stock. A more sound approach to the vulnerability estimation based on a fully probabilistic analysis of the available taxonomy is currently undergoing.

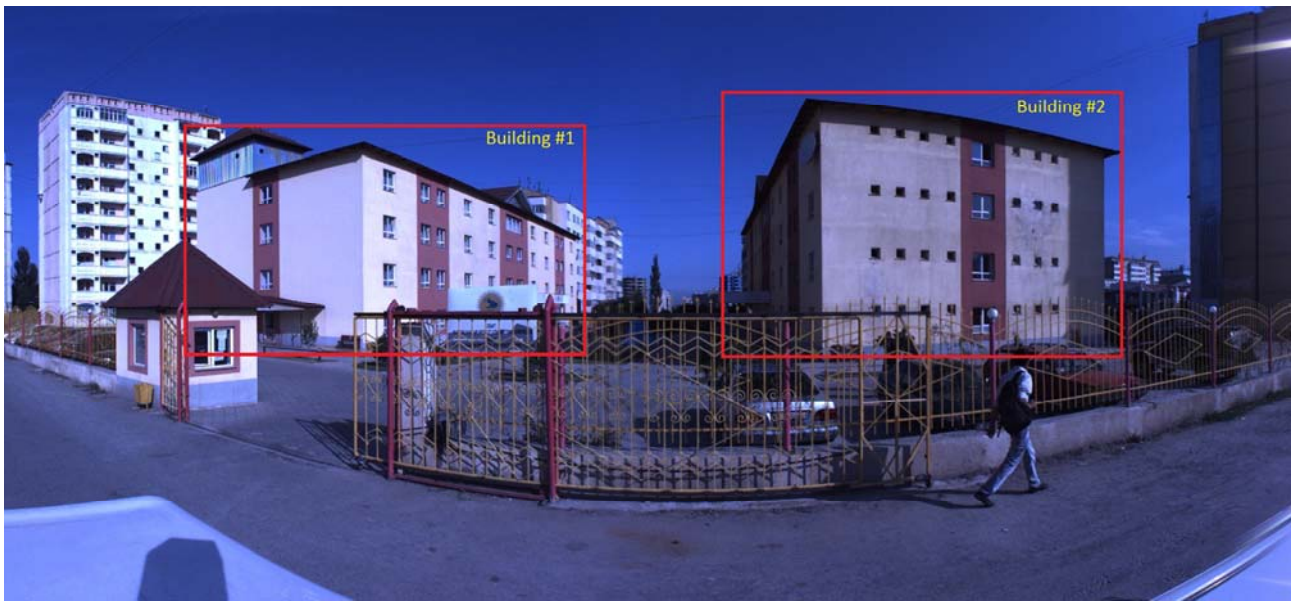

Fig. 11. Building #1 and #2 as captured by the omnidirectional camera.

Fig. 12. Building #3 as captured by the omnidirectional camera.

Fig. 13. Buildings #4 and #5 as captured by the omnidirectional camera.

7 Conclusions

The approach outlined within this paper allows for a fast and systematic data acquisition and analysis process for a multi-scale building inventory estimation. The integrated combination of satellite remote sensing and ground-based omnidirectional imaging provided a rich visual description of the urban environment. It therefore overcomes the limitations of purely satellite based approaches. By joining the advantages of the multiple imaging sources within the framework of an integrated sampling scheme, the proposed methodology is able to cope with the increasing spatio-temporal variability in present-day cities.

The case study of Bishkek showed that an initial analysis of medium-resolution satellite images from Landsat can provide a rapid standardized and transferable way to suitably partition a previously unknown city into homogeneous urban structure types. It therefore allowed for a systematic stratified sampling to identify representative sample areas for a local assessment at building scale. Therefore, acquisition costs and processing time could be reduced, because the required geographical extent is narrowed and only the necessary high-resolution data is acquired and processed. For Bishkek, a significant reduction of the geographical extent from 235 km² (total built-up area) to 12.3 km² (total sample area) could be achieved in a guided and meaningful way. Moreover, the analysis of medium-resolution satellite images allowed for an initial assessment of vulnerability-related features at block scale. For Bishkek, LULC classification showed a clear dominance of 1-2 storey apartment houses, which are mainly classified as highly vulnerable (A to B following the EMS-98 vulnerability classification) by local engineers. In combination with the results of the change detection analysis, it became clear that most of the newly built-up areas consist of this specific building type and that the urban sprawl is directed towards the most hazardous areas in the region close to the Issyk-Ata fault system. Therefore, a trend towards increasing seismic risk for the city of Bishkek could be already seen from a first regional assessment (see also [38]). Speed and direction of urban growth in recent years furthermore emphasise the need for a continuous update of the building inventory and vulnerability datasets for the city.

For a local assessment, ground-based omnidirectional image-capturing proved to be fast and easy to deploy in the field. The system can be operated even by non-skilled operators without affecting the expected outcomes. Routing and in-field car navigation allowed the effective navigation through the city without having prior knowledge of the place. During a one week field-trip in Bishkek, we were able to cover all of the pre-selected sample areas along the pre-calculated routes (125 km). To cover an area of similar size with a manual rapid visual screening by four skilled civil engineers would take about 9 weeks of fieldwork (personal communication, A. Duisheev, IntUIT, Bishkek). The captured omnidirectional video footage is a valuable and up-to-date source of diverse information about the current state of an urban area. Therefore, in addition to the proposed usage, it could also be used in the aftermath of an event to assess damages.

As a preliminary result for a small subset of buildings we showed, that based on a fully automatic processing of the captured omnidirectional images, it is possible to extract georeferenced information about geometrical and structural features of buildings. In combination with the outputs of suitable analyses of satellite images, these methodologies allowed to compile a multi-parameter database of inventory features. The automatically extracted features coming from multiple imaging sources in combination with information coming from the WHE allowed for a first vulnerability classification of the observed buildings according to EMS-98. However, to improve and further automatise this process more research is necessary. To strengthen the decision for a certain vulnerability class more inventory features (e.g. detection of soft-storeys, regularity and symmetry in shape, wall openings) need to be extracted from the images and further information about construction practises and the behaviour of different building types under earthquake ground-motion coming from local experts or external data sources needs to be taken into account. In the context of data integration and vulnerability classification the use of Bayesian networks seems a promising approach, which would also allow to account for uncertainties. It should furthermore be noted that a ground-based local assessment is not necessarily limited to an analysis of image data

only. Within the proposed approach, a local assessment could be extended to a further sampling level, where representative building samples are selected on the basis of the results of the high-resolution image analysis. The sampled buildings could than be further analysed from outside and inside by structural engineers following established standards such as the ASCE/SEI 31-03 seismic evaluation of existing buildings [41] to further enhance the quality of the inventory data.
Due to the high temporal resolution of the input data and the speed of the ground-based data-capturing, it would be possible to regularly update the inventory database in a standardized and guided way. Moreover, due to the structure of the sampling approach there is the possibility to extrapolate the building scale information to block scale and therefore provide with an estimate of the building inventory for the whole city. Such a city-wide inventory estimate for Bishkek on a block scale is not existing until now. The proposed approach makes use of both supervised and unsupervised processing, and in order to be fully effective it must be complemented by local expert knowledge and tailored to the specific application. However, it needs to be pointed out that almost no technical knowledge of data mining or advanced image processing is required in order to fully exploit its potential advantages.
The proposed methods and tools are developed on an open-source basis and low-cost, globally available data sources are preferred. This allows for a high degree of transferability and usability. It may also help to empower less equipped institutions in developing countries, which are especially vulnerable to natural hazards, to perform the necessary risk-preventive analysis by themselves. Future research will include automated vulnerability classification of the identified buildings considering uncertainties and the extrapolation of the results from building scale to block scale to cover the whole town. Furthermore, it is planned to combine a probabilistic vulnerability map for Bishkek with the results of seismic hazard analysis [42] to update and improve risk scenarios for the city [38] in a probabilistic framework.

8 Acknowledgements

This research has been funded by CEDIM (Center for Disaster Management and Risk Reduction), PROGRESS (Georisiken im Globalen Wandel) and Helmholtz-EOS (Earth Observation System). The authors would like to thank CAIAG (Central Asian Institute for Applied Geoscience) and IntUIT (International University for Innovation Technologies) for their support during the ground-based data-capturing.

9 References

[1] R. Bilham, The seismic future of cities, Bulletin of Earthquake Engineering 7:4 (2009) 839–887.
[2] G. M. Calvi, R. Pinho, G. Magenes, J. J. Bommer, L. F. Restrepo-Velez, H. Crowley, Development of seismic vulnerability assessment methodologies over the past 30 years, ISET journal of Earthquake Technology 43:472 (2006) 75–104.
[3] FEMA 154, Federal Emergency Management Agency, Rapid visual screening of buildings for potential seismic hazards: a handbook, second ed., ATC, Washington, 2002.
[4] A. Fekete, M. Damm, J. Birkmann, Scales as a challenge for vulnerability assessment, Natural Hazards 55 (2010) 729-747.
[5] Global Earthquake Model (Online), accessed 08.07.2011 (http://www.globalquakemodel.org).
[6] H. Taubenböck, T. Esch, A. Roth, An urban classification approach based on an object-oriented analysis of high resolution satellite imagery for a spatial structuring within urban areas, 1st EARSeL Workshop of the SIG Urban Remote Sensing, Berlin 2006.
[7] K. Saito, R. Spence, C. Going, M. Markus, Using high-resolution satellite images for post-earthquake building damage assessment: A study following the 26.1.01 Gujurat earthquake, Earthquake Spectra 20:1 (2004) 145-170.
[8] H. Taubenböck, C. Münch, J. Zschau, A. Roth, L. Stempniewski, S. Dech, H. Mehl, Assessing

building vulnerability using synergistically remote sensing and civil engineering, in: A. Krek, M. Rumor, S. Zlatanova, M. Fendel (Eds.), Urban and Regional Data Management, Taylor & Francis Group, London, 2009, pp. 287-300.
[9] H. Taubenböck, T. Esch, M. Wurm, M. Thiel, T. Ullmann, A. Roth, M. Schmidt, H. Mehl, S. Dech, Urban structure analysis of mega city Mexico city using multi-sensoral remote sensing data, Proceedings of SPIE, Cardiff 2008.
[10] F. Yamazaki, T. Vu, M. Matsuoka, Dual-scale approach for detection of tsunami-affected areas using optical satellite images, International Journal of Remote Sensing 28:13-14 (2007) 2995-3011.
[11] A. Torii, M. Havlena, T. Pajdla, From google street view to 3D city models, IEEE 12th International Conference on Computer Vision Workshops, Kyoto 2009.
[12] S. Teller, Toward urban model acquisition from geo-located images, Proceedings of Pacific Graphics, Singapore 1998.
[13] U. Neumann, L. Wand, S. You, Large-scale urban modeling by combining ground level panoramic and aerial imagery, Proceedings of the Third International Symposium on 3D Data Processing, Visualization, and Transmission, Chapel Hill 2006.
[14] T. Blaschke, Object based image analysis for remote sensing, ISPRS Journal of Photogrammetry and Remote Sensing 65 (2010) 2–16.
[15] P. Felzenzwalb, D. Huttenlocher, Efficient graph-based image segmentation, International Journal of Computer Vision 59 (2004) 167-181.
[16] V. Vapnik, The nature of statistical learning theory, second ed., Springer, New York, 2000.
[17] C. J. C. Burges, A tutorial on support vector machines for pattern recognition, Data mining and knowledge discovery 2 (1998) 121–167.
[18] H. Yang, B. Ma, Q. Du, and C. Yang, Improving urban land use and land cover classification from high-spatial-resolution hyperspectral imagery using contextual information, Journal of Applied Remote Sensing 4:1 (2010) 041890.
[19] T. Lillesand, R. Kiefer, J. Chipman, Remote Sensing and Image Interpretation, sixth ed., Wiley, Sussex, 2008.
[20] R. Haralick, K. Shanmugam, I. Dinstein, Textural features for image classification, IEEE Transactions on system, man and cybernetics 3:6 (1973) 610-621.
[21] D. Lu, P. Mausel, E. Brondizio, E. Moran, Change detection techniques, International Journal of Remote Sensing 25 (2004) 2365–2401.
[22] J. Mas, Monitoring landcover changes: a comparison of change detection techniques, International Journal of Remote Sensing 20 (1999) 139-152.
[23] G. Grünthal, R. Musson, J. Schwarz, M. Stucchi, European macroseismic scale 1998 (EMS-98), Cahiers du Centre Européen de Géodynamique et de Séismologie 15 (1998).
[24] W. G. Cochran, Sampling techniques, third ed., Wiley, Sussex, 1977.
[25] G. van Belle, D. C. Martin, Sample size as a function of coefficient of variation and ratio of means, The American Statistician 47:3 (1993) 165-167.
[26] OpenStreetMap (Online), accessed 21.11.2010 (http://www.openstreetmap.org).
[27] J. K. Lenstra, A. H. G. Rinnooy Kan, Some simple applications of the travelling salesman problem, Operational Research Quarterly 26:4 (1975) 717-733.
[28] E. W. Dijkstra, A note on two problems in connexion with graphs, Numerische Mathematik 1 (1959) 269–271.
[29] S. S. Lin and R. Bajcsy, Single-viewpoint, catadioptric cone mirror omnidirectional imaging theory and analysis, Journal of the Optical Society of America 23:12 (2006) 2997-3015.
[30] H. Haggrén, H. Hyyppä, O. Jokinen, A. Kukko, M. Nuikka, T. Pitkänen, P. Pöntinen, P. Rönnholm, Photogrammetric application of spherical imaging, Panoramic Photogrammetry Workshop, Dresden 2004.
[31] D. Maling, Coordinate systems and map projections, Pergamon Press, Oxford, 1992.
[32] A. Torii, A. Imiya, and N. Ohnishi, Two-and three-view geometry for spherical cameras, Proceedings of the Sixth Workshop on Omnidirectional Vision, Camera Networks and Non-

classical Cameras, Beijing 2005.
[33] I. Stratmann, Omnidirectional imaging and optical flow, Proceedings of the Third Workshop on Omnidirectional Vision, Kopenhagen 2002.
[34] Z. Arican, P. Frossard, Dense depth estimation from omnidirectional camera, Signal Processing Laboratory LTS4 Technical Report, no. TR-LTS-2009-006.
[35] M. Mainberger, A. Bruhn, and J. Weickert, Is dense optic flow useful to compute the fundamental matrix?, Image Analysis and Recognition (2008) 630–639.
[36] B. K. P. Horn, Recovering baseline and orientation from essential matrix, Journal of the Optical Society of America (1990).
[37] K. Abdrakhmatov, H.B. Havenith, D. Delvaux, D. Jongmans, P. Trefois, Probabilistic PGA and arias intensity maps of Kyrgyzstan (Central Asia), Journal of Seismology 7 (2003) 203–220.
[38] D. Bindi, M. Mayfield, S. Parolai, S. Tyagunov, U. Begaliev, K. Abdrakhmatov, B. Moldobekov, J. Zschau, Towards an improved seismic risk scenario for Bishkek, Kyrgyz Republic, Soil Dynamics and Earthquake Engineering 31:3 (2011) 521-525.
[39] M. Erdik, T. Rashidov, E. Safak, A. Turdukulov, Assessment of seismic risk in Tashkent, Uzbekistan and Bishkek, Kyrgyz Republic, Soil Dynamics and Earthquake Engineering 25 (2005) 473-486.
[40] World Housing Encyclopedia (Online), accessed 10.04.2011 (http://www.world-housing.net).
[41] ASCE/SEI 31-03, American Society of Civil Engineers, Seismic evaluation of existing buildings, ASCE, Reston, 2003.
[42] S. Parolai, S. Orunbayev, D. Bindi, A. Strollo, S. Usupayev, M. Picozzi, D. Di Giacomo, E. Augliera, C. Milkereit, B. Moldobekov, J. Zschau, Site effect assessment in Bishkek (Kyrgyzstan) using earthquake and noise recording data, Bulletin of the Seismological Society of America 100:6 (2010) 3068-3082.